Sol–gel preparation of spherical γ-Al_2O_3 with macro-mesopores as an efficient adsorbent for acid fuchsin

Tiantian Zhang, Xiulan Xin ✉, Hongqin Liu, Nan Song, Yan Wang, Yige Shi, Yuqing Cheng

School of Light Industry, Beijing Technology and Business University, Beijing 100048, People's Republic of China
✉ *E-mail: xinxl2007@126.com*

Published in Micro & Nano Letters; Received on 10th May 2020; Revised on 7th August 2020; Accepted on 31st August 2020

Spherical gamma-alumina (γ-Al_2O_3) has a wide range of applications in the field of adsorption due to its low bulk density, larger pore size, higher strength and thermal stability. In this study, spherical γ-Al_2O_3 with macro-mesopores was prepared with isopropanol aluminium as the aluminium source via a sol–gel process. Spherical γ-Al_2O_3 was characterised by means of nitrogen adsorption and desorption curve, scanning electron microscope, transmission electron microscope, X-ray diffraction and so on. The adsorption performance of the prepared spherical γ-Al_2O_3 was studied by probe experiment of adsorption of acid fuchsin (AF) solution. The results showed that the spherical γ-Al_2O_3, which was prepared under the condition of hydrolysis time of 1 h, hydrolysis temperature of 85°C, ageing temperature of 95°C and ageing time of 7 h, had the strongest adsorption capacity for AF, and the adsorption efficiency could reach 96.24% in 40 mg/l AF solution. In addition, after six cycles of use, the spherical γ-Al_2O_3 had no damage and the adsorption efficiency still could reach 88.40%. This work provides a feasible method for the preparation of spherical γ-Al_2O_3, and could also help to understand the connection between its textural properties and adsorption performance.

1. Introduction: As we all know, in recent years, the problem of freshwater resources has been one of the important factors affecting human health and restricting social development. Especially, in some industrial production, such as textile manufacturers, paper industry, plastic production enterprises and so on, a large number of coloured wastewater containing kinds of various dyes and pigments will inevitably be discharged [1, 2]. However, dyes and pigments, as the main pollutants in wastewater, which have complex aromatic molecular structures, are difficult to degrade [3]. Therefore, the treatment of various dyes or pigments wastewater can effectively reduce the waste of water. It is particularly urgent and important to develop the corresponding technology with low cost, simple and efficient processes [4].

At present, the main methods to remove pollutants in wastewater include adsorption method [5, 6], biological decolourisation method [7, 8], photocatalytic degradation method [9], ultrasonic degradation method [10], advanced microwave enhanced oxidative program degradation method [4] and so on. Among these methods, the biological degradation method needs to protect the activity of the strain and requires higher culture environment [7], the ultrasonic degradation method needs to make use of the synergistic effect of hydrogen peroxide, which has strong oxidation and needs to be sealed [10]. While the adsorption method is simple, and different adsorbents have different adsorption effects.

Common adsorbents include activated carbon [11, 12], ferromagnetic metals [13–15], metal oxides [16–21] and so on. Spherical gamma-alumina (γ-Al_2O_3), which has a large specific surface area (SSA) and mechanical strength and good heat resistance, can be used as adsorbent and catalyst support [22–26]. Spherical γ-Al_2O_3 also plays an important role in mass and heat transfer. Elsayed *et al.* [27] and Hoseinzadeh *et al.* [28] studied the role of alumina in thermal energy. The preparation of spherical γ-Al_2O_3 has been divided into two distinct techniques: snowball granulation [29] and liquid phase moulding [30]. The spherical γ-Al_2O_3 prepared by the first method has some defects, such as low mechanical resistance, poor attrition resistance and randomly granule size distribution. Compared to the former, the obtained granules by the later have a uniform granule size, excellent mechanical properties, controlled pore size and distribution. Generally, liquid phase moulding methods include oil ammonia column formation [31, 32], hot oil formation [33] and spray drying [34]. The oil ammonia column method has the advantages of simple process, safety, low price and recyclability, and has many industrial applications. Hoseinzadeh *et al.* [35] successfully synthesised WO_3 particles by sol–gel method. Zhang *et al.* [36] reported that γ-Al_2O_3 calcined at 500°C was used to adsorb 100 mg/l of acid fuchsin (AF) solution, and the removal efficiency was only about 35%. Ramezani *et al.* [37] studied the effect of interface roughness and temperature on the spin filtration process. Herein, a sol was prepared by hydrolysis and ageing with aluminium isopropoxide as a raw material, and then the spherical γ-Al_2O_3 was obtained through the process of an oil ammonia column method and calcination. The effects of temperatures or time of hydrolysis and ageing on the morphology and textural properties of the materials have been studied. The adsorption performance of spherical γ-Al_2O_3 was studied by probe experiment of adsorption of AF solution, which revealed their potential applications as adsorbent materials for wastewater purification. The relationship between the textural properties and the adsorption performance based on spherical γ-Al_2O_3 adsorbents was discussed.

2. Experimental procedure

2.1. Preparation of spherical γ-Al_2O_3: For a standard synthesis, 10.21 g of aluminium isopropoxide and 18.43 g of distilled water were placed in the three-necked flask, and hydrolysed at the certain temperature for a certain time. All compositions are given in Tables 1 and 2. Then, 3.92 ml (1 mol/l) of dilute nitric acid was added and gel ageing in a certain temperature for a certain time was done to obtain an aluminium sol with the certain viscosity. The pH of aluminium sol is 3.5 ± 0.5. Spherical γ-Al_2O_3 precursor was prepared by oil-ammonia column shaping method. After drying at room temperature (25 ± 1°C) for 24 h, and drying at 110°C for 8 h, calcination followed at 600°C for 4 h to obtain spherical γ-Al_2O_3.

2.2. Adsorption experiment: About 50 mg of sorbent was introduced into a 20 ml vial containing 10 ml of a 40 mg/l AF solution, and left at room temperature. The residual AF (η) concentration in the solution was measured using an ultraviolet (UV) visible spectrophotometer every 1 h. A full spectrum scan (Fig. 1*b*) showed that the maximum absorption wavelength (λ) of AF was 545 nm.

Table 1 SSA, PD and PV data of 25 groups of orthogonal experimental samples

Number	Hydrolysis time, min	Hydrolysis temperature, °C	Ageing time, h	Ageing temperature, °C	SSA, m^2/g	PV, cm^3/g	PD, nm
1	5	55	1	85	275.25	0.45	6.55
2	5	65	3	95	261.92	0.43	6.36
3	5	75	5	105	244.29	0.43	6.78
4	5	85	10	115	252.90	0.45	6.78
5	5	95	20	125	245.55	0.48	7.46
6	15	55	3	105	258.10	0.41	6.09
7	15	65	5	115	246.24	0.44	6.91
8	15	75	10	125	240.38	0.44	7.07
9	15	85	20	85	252.76	0.46	6.93
10	15	95	1	95	321.25	0.54	6.45
11	30	55	5	125	244.60	0.41	6.49
12	30	65	10	85	260.04	0.41	6.13
13	30	75	20	95	243.61	0.44	7.00
14	30	85	1	105	263.82	0.45	6.85
15	30	95	3	115	257.37	0.45	6.92
16	60	55	10	95	266.89	0.42	6.30
17	60	65	20	105	258.03	0.47	7.26
18	60	75	1	115	256.11	0.43	6.69
19	60	85	3	125	250.60	0.44	6.99
20	60	95	5	85	259.07	0.45	6.93
21	120	55	20	115	260.15	0.45	6.85
22	120	65	1	125	263.31	0.46	6.95
23	120	75	3	85	254.99	0.42	6.58
24	120	85	5	95	264.70	0.43	6.53
25	120	95	10	105	253.44	0.43	6.82
x^a_{1j}	264.21	265.69	279.00	264.43	6487.63c		
x^a_{2j}	275.55	263.84	260.92	278.59			
x^a_{3j}	260.11	254.03	258.09	260.05			
x^a_{4j}	258.14	261.23	261.08	258.94			
x^a_{5j}	259.32	272.54	258.24	255.31			
R^b_j	17.41	12.95	2.99	9.12			

Table 2 SSA, PD and PV data of: γ-Al_2O_3-20, γ-Al_2O_3-24, different hydrolysis time, different ageing time and commercially available spherical alumina (γ-Al_2O_3-ss)

Sample name	Hydrolysis time, min	Hydrolysis temperature, °C	Ageing time, h	Ageing temperature, °C	SSA, m^2/g	PV, cm^3/g	PD, nm	Adsorption efficiency, %
γ-Al_2O_3-20	60	95	5	85	259.07	0.45	6.93	86.29
γ-Al_2O_3-24	120	85	5	95	264.70	0.43	5.19	—
γ-Al_2O_3-30 min	30	85	6	95	263.67	0.45	6.76	—
γ-Al_2O_3-60 min	60	85	6	95	265.50	0.46	6.80	95.32
γ-Al_2O_3-90 min	90	85	6	95	240.11	0.42	6.97	—
γ-Al_2O_3-120 min	120	85	6	95	249.11	0.43	6.89	—
γ-Al_2O_3-6 h	60	85	6	95	261.88	0.46	7.17	—
γ-Al_2O_3-7 h	60	85	7	95	262.57	0.48	7.38	96.24
γ-Al_2O_3-8 h	60	85	8	95	243.17	0.44	7.36	—
γ-Al_2O_3-9 h	60	85	9	95	253.27	0.44	7.02	—
γ-Al_2O_3-10 h	60	85	10	95	250.76	0.42	6.65	—
γ-Al_2O_3-ss	—	—	—	—	195.55	0.50	7.49	74.24

The adsorption efficiency (R, %) was calculated from the absorbance of AF (η) at 545 nm by the following formula:

$$R = \left[(A_0 - A_t)/A_0\right] \times 100\% \quad (1)$$

where A_0 (mg/l) was the initial absorbance value of the AF solution and A_t (mg/l) was the residual solution absorbance value at time t [36].

Spherical γ-Al_2O_3 recycling experiment: the adsorbed spherical γ-Al_2O_3 was taken out and put into an oven, dried at 110°C for 8 h, and calcined followed at 600°C for 4 h to obtain spherical γ-Al_2O_3.

2.3. Characterisation: The thermal behaviour of precursor has been investigated by the use of thermal gravimetric analysis (TGA) and differential thermal (DTG) analysis (MS3000, Mettler Toledo, China) [37]. The X-ray diffraction (XRD) patterns were recorded on Bruker Axs diffractometer (Germany) using Cu Kα radiation as the X-ray source in the 2θ range of 10–80°. The Fourier transform infrared (FTIR) spectra of the samples were recorded on Nicolet Avatar 370 spectrometer in the range of 400–4000 cm^{-1}. The samples have been well mixed with the dried KBr powder, pressed to form disk tablets and used for measurements. Scanning electron microscopy (SEM) analysis was performed using a Zeiss Supra 55 microscope at an acceleration voltage of 1 kV [38].

doi: 10.1049/mnl.2020.0271

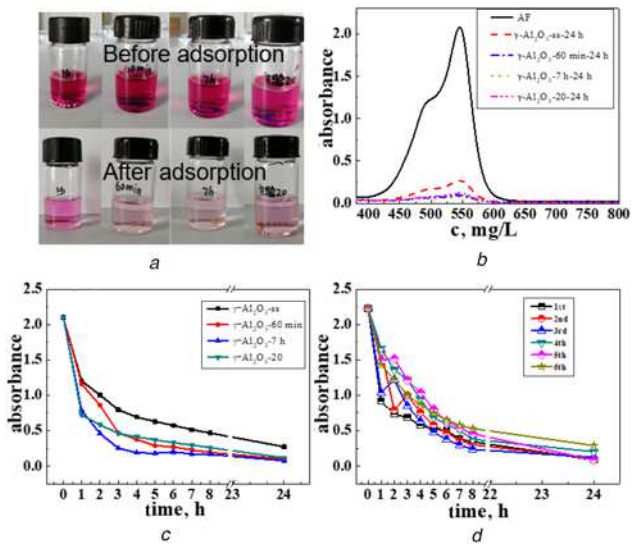

Fig. 1 *Adsorption effect of*
a Photograph of different γ-Al_2O_3 before and after adsorption in AF solution (40 mg/l)
b Absorbance changes of UV absorption spectra from different γ-Al_2O_3 along with λ
c Time at 545 nm in AF (40 mg/l)
d Absorbance changes of UV absorption spectra from γ-Al_2O_3-7 h along with time for six recycle tests at 545 nm in AF (40 mg/L)

Nitrogen isothermal sorption measurements were carried out on a Micrometrics TRISTAR 3000 analyser at −196°C. The samples were first outgassed at 300°C with a vacuum degree of 10^{-2} Torr for more than 3 h prior to nitrogen adsorption–desorption measurement. Brunauer–Emmett–Teller method ($0.01 < P/P_o < 0.1$) was utilised to calculate the SSAs. The pore size distribution was derived from the desorption branch, using the Barrett–Joyner–Halenda method.

3. Results and discussion

3.1. Characterisation of the γ-Al_2O_3: Taking the four factors of hydrolysis time, hydrolysis temperature, ageing time and ageing temperature and five levels of each factor into consideration, we designed 25 orthogonal experiments to investigate the main factors affecting the SSA and pore structure of the samples. The samples were named γ-Al_2O_3-1, γ-Al_2O_3-2, γ-Al_2O_3-3, γ-Al_2O_3-4, …, γ-Al_2O_3-25 according to the sample serial number. Table 1 gives the detailed information on the SSA, pore volume (PV) and pore diameter (PD) of all the samples prepared in the 25 groups of experiments. It can be seen that all the samples have large SSA (>240 m^2/g), average PV (>0.4 cm^3/g) and average pore size (>6 nm). In addition, through the orthogonal calculation based on the SSA, we conclude that hydrolysis temperature and ageing temperature are two important factors. Digital microscope photos (DMP) (Fig. 2) distinctly show all the samples exhibiting regular spherical structure apart from the γ-Al_2O_3-10, which were broken after calcination. The morphology and microstructures of the obtained samples were studied by SEM, and the sample with the largest number of micron-sized pores would be selected as the adsorbent for the adsorption experiment. As seen in Fig. 3, according to the number of micron-sized pores, γ-Al_2O_3-20 was selected as a group of adsorbents for the adsorption experiment.

In addition, in order to explore the best experimental conditions, a single factor experiment was designed, the hydrolysis time or ageing time was as single-factor variable with the fixed hydrolysis temperature was 85°C and the ageing temperature was 95°C. According to the different hydrolysis time, the samples were

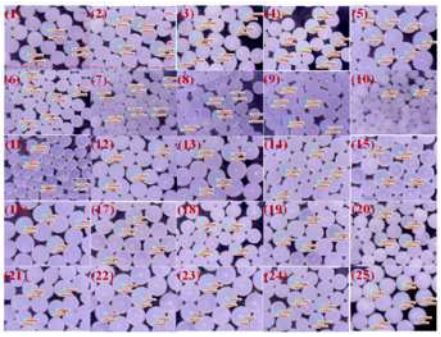

Fig. 2 *DMP of different γ-Al_2O_3 from 25 sets of orthogonal experiments*

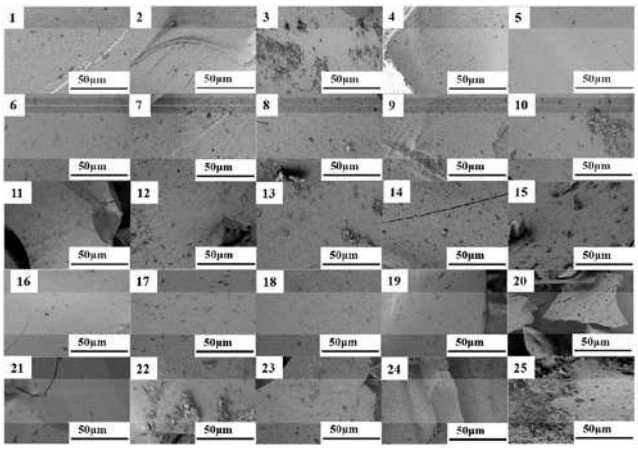

Fig. 3 *SEM of different γ-Al_2O_3 from 25 sets of orthogonal experiments*

named γ-Al_2O_3-30 min, γ-Al_2O_3-60 min, γ-Al_2O_3-90 min, γ-Al_2O_3-120 min. Based on the SEM micrographs (Fig. 4), γ-Al_2O_3-60 min with the most micron-sized pores was selected for the adsorption experiment. The calcined samples were named γ-Al_2O_3-6 h, γ-Al_2O_3-7 h, γ-Al_2O_3-8 h, γ-Al_2O_3-9 h, γ-Al_2O_3-10 h according to the different ageing time. Similarly, according to the SEM micrographs (Fig. 5), γ-Al_2O_3-7 h with the most micron-sized pores was selected for the adsorption experiment. The morphology features of all the samples exhibited regular and millimetre-sized spherical structure, which also can be found in Figs. 2, 6 and 7.

TGA and DTG analysis of the precursor of γ-Al_2O_3-7 h (7 h-precursor) were used to clarify the change of components of the materials investigated above during the calcination process. From Fig. 8, it can be seen that three thermal decomposition

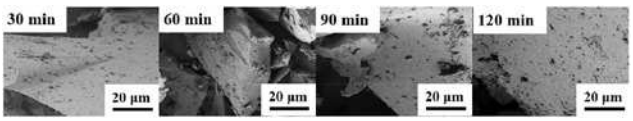

Fig. 4 *SEM of γ-Al_2O_3 with different hydrolysis time and same ageing time 6 h*

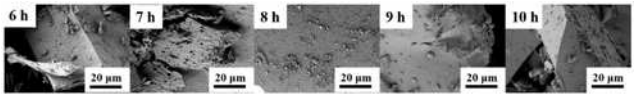

Fig. 5 *SEM of with different ageing time and same hydrolysis time 60 min*

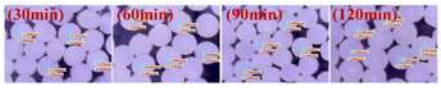

Fig. 6 *DMP of γ-Al_2O_3 with different hydrolysis time and same ageing time 6 h*

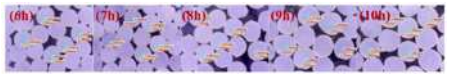

Fig. 7 *DMP of γ-Al_2O_3 with different ageing time and same hydrolysis time 60 min*

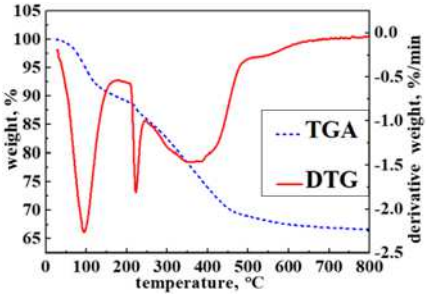

Fig. 8 *TG and DTG of 7 h-precursor in air (the hydrolysis temperature was 85°C, the hydrolysis was 60 min, the ageing temperature was 100°C, and the sol was aged for 7 h)*

steps were observed. Due to the desorption of adsorbed water, the first thermal decomposition occurred before 150°C, the second step was located at 200–250°C, which was due to the desorption of crystal water and a small amount of alcohol, and the third was at 260–600°C, from which the 7 h-precursors removes structured water and transforms into γ-Al_2O_3. It can also be seen that the weight of the precursor is basically unchanged between 600 and 800°C, which reveals that there is no endothermic and exothermic situation. It also can be concluded that there was no crystal phase transformation. Therefore, the spherical sample was obtained by calcining the dried pellets at 600°C. The XRD patterns (Fig. 9) of the samples after calcination showed that there were diffraction peaks at (220), (311), (222), (400), (511) and (440), indicating that the obtained spherical alumina sample had a γ-Al_2O_3 structure (JCPDS no.29-0063) [32]. Comparing the XRD diffraction peak intensities of the samples prepared under different ageing time, as shown in Fig. 9*b*, it is found that the γ-Al_2O_3-60 min and γ-Al_2O_3-120 min exhibited similar diffraction peaks in intensity.

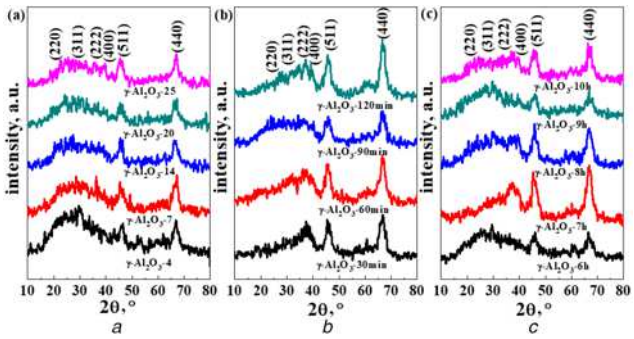

Fig. 9 *XRD patterns of different spherical γ-Al_2O_3*
a γ-Al_2O_3-4; γ-Al_2O_3-7; γ-Al_2O_3-14; γ-Al_2O_3-20; γ-Al_2O_3-25
b γ-Al_2O_3-30 min; γ-Al_2O_3-60 min; γ-Al_2O_3-90 min; γ-Al_2O_3-120 min
c γ-Al_2O_3-6 h; γ-Al_2O_3-7 h; γ-Al_2O_3-8 h; γ-Al_2O_3-9 h; γ-Al_2O_3-10 h

As illustrated in Fig. 9*c*, as the ageing time increases, the peak of the alumina upshifted and became stronger firstly and then decreased, which indicted that γ-Al_2O_3-7 h possessed the largest crystal phase strength. FTIR spectra (Fig. 10) showed that after calcination at 600°C, the Al–O–Al band absorption peak of γ-Al_2O_3 appeared in the range of 500–800 cm^{-1}, and –OH absorption peak of H_2O appeared at 1630 cm^{-1}, indicating that the prepared samples had a γ-Al_2O_3 crystal structure and strong water absorption capacity [39].

The SEM micrographs showed that most of the experimental samples had no micron-sized pore structures without the addition of any pore-forming agent (Figs. 3–5). However, the samples γ-Al_2O_3-20, γ-Al_2O_3-60 min and γ-Al_2O_3-7 h showed micron-sized pore structures, as shown in Fig. 11. The cross-sections of samples γ-Al_2O_3-24, γ-Al_2O_3-120 min and γ-Al_2O_3-8 h did not show micron-sized pore structures (Fig. 12). The reason may be that the hydrolysis time or ageing time affected the pore formation process of the aluminium sol, and the pore size kept shrinking along with the extension of the time, resulting in the change of the pore structure.

We can see from Fig. 13 that the samples γ-Al_2O_3-20, γ-Al_2O_3-60 min and γ-Al_2O_3-7 h had uniform grain distribution, and the average pore sizes were 6.93, 6.80 and 7.38 nm, respectively. While for the control group γ-Al_2O_3-24, γ-Al_2O_3-120 min and

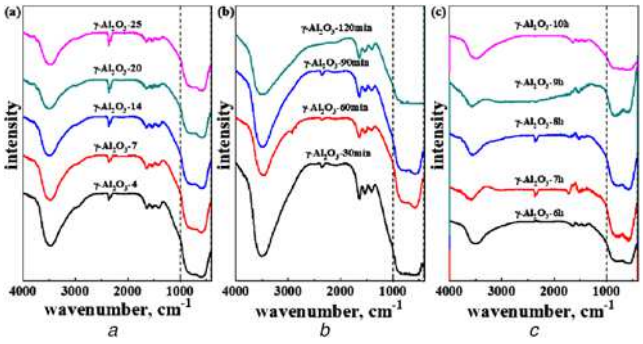

Fig. 10 *FTIR spectra of different spherical γ-Al_2O_3*
a γ-Al_2O_3-4; γ-Al_2O_3-7; γ-Al_2O_3-14; γ-Al_2O_3-20; γ-Al_2O_3-25
b γ-Al_2O_3-30 min; γ-Al_2O_3-60 min; γ-Al_2O_3-90 min; γ-Al_2O_3-120 min
c γ-Al_2O_3-6 h; γ-Al_2O_3-7 h; γ-Al_2O_3-8 h; γ-Al_2O_3-9 h; γ-Al_2O_3-10 h

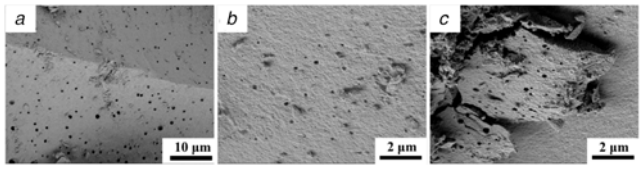

Fig. 11 *SEM micrographs of*
a γ-Al_2O_3-20
b γ-Al_2O_3-60 min
c γ-Al_2O_3-7 h

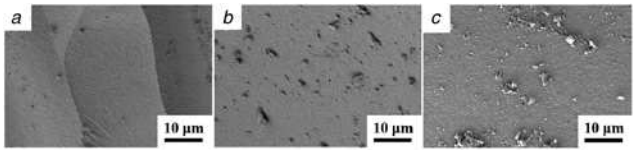

Fig. 12 *SEM of*
a γ-Al_2O_3-24
b γ-Al_2O_3-120 min
c γ-Al_2O_3-8 h

doi: 10.1049/mnl.2020.0271

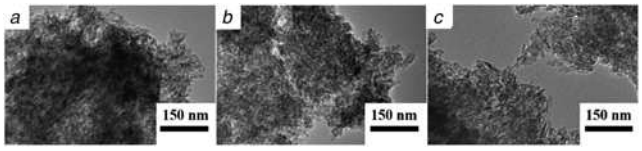

Fig. 13 *Transmission electron micrographs of*
a γ-Al_2O_3-20
b γ-Al_2O_3-60 min
c γ-Al_2O_3-7 h

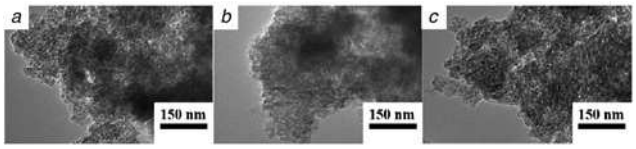

Fig. 14 *Transmission electron microscopy of*
a γ-Al_2O_3-24
b γ-Al_2O_3-120 min
c γ-Al_2O_3-8 h

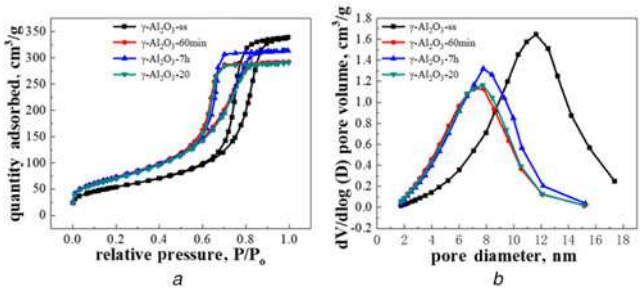

Fig. 15 *Pore structure of*
a Nitrogen sorption isotherms
b Pore size distribution of γ-Al_2O_3-20, γ-Al_2O_3-60 min, γ-Al_2O_3-7 h

γ-Al_2O_3-8 h shown in Fig. 14, the micro-grain distribution was rather chaotic. By comparison, it is found that samples with uniform grain distribution were more likely to form micron-sized pore structures, while samples with chaotic grain distribution were denser when they are stacked, and were not easy to form micron-sized pore structures. Therefore, by selecting appropriate experimental conditions, γ-Al_2O_3 samples with different pore sizes can be obtained.

The structural characteristics of the samples obtained by nitrogen adsorption–desorption isotherms were listed in Tables 1 and 2. From the average pore size PD value, it can be seen that all samples have mesoporous structure with different sizes. Based on the IUPAC classification, the mesoporous structure was determined by a type IV isotherm obtained from the synthesised γ-Al_2O_3, which can be seen from Fig. 15*a*. As shown in Fig. 15*b*, the spherical γ-Al_2O_3 product forms a wide pore size distribution with the pore size ranging from 2 to 16 nm, which can establish more possibilities for adsorption sites and promote adsorption performance.

3.2. Adsorption studies: The adsorption behaviour of the sample γ-Al_2O_3 in AF solution was studied to evaluate its potential application in the treatment of coloured water. As seen in Fig. 1*a*, the adsorption efficiency of the spherical sample γ-Al_2O_3-60 min, γ-Al_2O_3-7 h and γ-Al_2O_3-20 was higher than the commercial spherical γ-Al_2O_3-ss, which was content with the absorption spectra. The adsorption of different γ-Al_2O_3 for AF was shown in

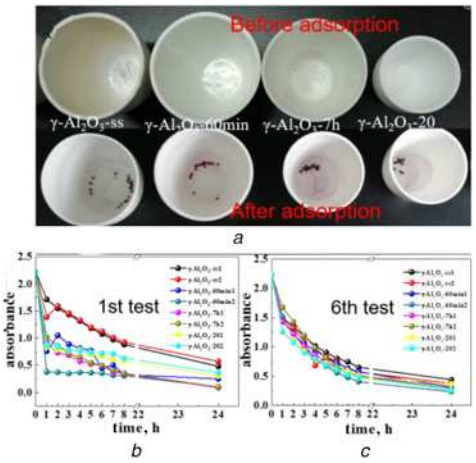

Fig. 16 *Repeat six times of*
a Photograph of different γ-Al_2O_3 before and after adsorption in AF solution
b, *c* Absorbance changes at 545 nm of adsorption of AF (40 mg/l) by different γ-Al_2O_3 which all use two sets of samples for 24 h for the first and sixth tests

Fig. 1*b*. The results showed that the absorbance of the 40 mg/l AF solution was 2.020, and the absorbance values of the four kinds of spherical γ-Al_2O_3 were greatly reduced after 24 h (Fig. 16). Among them, the sample γ-Al_2O_3-7 h possessed the greatest adsorption efficiency of 96.24%, which was much higher than γ-Al_2O_3-ss of 86.53%. The absorbance values of the four kinds of spherical γ-Al_2O_3 also exhibited similar behaviours along with time in Fig. 1*c*. The adsorption process can be divided into two stages. Within the first 1 h, AF was quickly adsorbed to γ-Al_2O_3-ss, γ-Al_2O_3-60 min, γ-Al_2O_3-7 h and γ-Al_2O_3-20. In the second stage, AF was slowly adsorbed within 1–24 h. After 24 h, the self-made spherical γ-Al_2O_3 sample absorbed AF solution with a lower absorption value than the commercially available γ-Al_2O_3-ss. It can be inferred that the AF was absorbed through amount of exposed macropores and accessible micropores in a short time, and enters the complex micropores inside the γ-Al_2O_3 slowly.

After six cycles of test, as shown in Fig. 16, the samples γ-Al_2O_3-60 min, γ-Al_2O_3-7 h and γ-Al_2O_3-20 all still maintain a spherical structure without damage and excellent adsorption efficiency, especially the adsorption rate of sample γ-Al_2O_3-7 h reached at 88.40% (Fig. 1*d*). As listed in Table 1, by comparing the samples with different textural properties and adsorption efficiency, it can be inferred that a larger SSA can provide more adsorption sites, thereby promoting the improvement of adsorption performance.

4. Conclusion: In summary, we prepared spherical γ-Al_2O_3 with macro-mesopores by a simple approach, and the hydrolysis and ageing time affected their SSA and pore size. The macro-mesopores structure was advantageous for the ion transmission, and more adsorption sites were created by large SSA for adsorption. The results showed that the spherical γ-Al_2O_3-7 h, which was prepared under the condition of hydrolysis time of 1 h, hydrolysis temperature of 85°C, ageing temperature of 95°C and ageing time of 7 h, had the strongest adsorption capacity for AF. Its SSA was 262.57 m^2/g, PV was 0.48 m^3/g and its adsorption efficiency in 40 mg/l AF solution was 96.24%, and it reached 88.40% after six cycles of testing. Therefore, this work provides important information for understanding the preparation of spherical γ-Al_2O_3 with excellent adsorption capabilities and reusability, and as adsorbents, it can also be further applied to other types of dye wastewater processing.

5. Acknowledgments: This work was supported by the Beijing Municipal Science and Technology Project (grant D17110500190000).

6 References

[1] Garg V.K., Kumar R., Gupta R.: 'Removal of malachite green dye from aqueous solution by adsorption using agroindustry waste: a case study of Prosopis cineraria', *Dyes Pigm.*, 2004, **62**, (1), pp. 1–10

[2] Banat I.M., Nigam P., Singh D., *ET AL.*: 'Microbial decolorization of textile-dye-containing effluents; a review', *Bioresour. Technol.*, 1996, **58**, (3), pp. 217–227

[3] Sun Q., Yang L.: 'The adsorption of basic dyes from aqueous solution on modified peat–resin particle', *Water Res.*, 2003, **37**, (7), pp. 1535–1544

[4] Zhang L., Zhou X.Y., Guo X.J., *ET AL.*: 'Investigation on the degradation of acid fuchsin induced oxidation by $MgFe_2O_4$ under microwave irradiation', *J. Mol. Catal. A, Chem.*, 2011, **335**, (1–2), pp. 31–37

[5] Burakov A.E., Galunin E.V., Burakova I.V., *ET AL.*: 'Adsorption of heavy metals on conventional and nanostructured materials for wastewater treatment purposes: a review', *Ecotoxicol. Environ. Saf.*, 2018, **148**, pp. 702–712

[6] Santhosh C., Velmurugan V., Jacob G., *ET AL.*: 'Role of nanomaterials in water treatment applications: a review', *Chem. Eng. J.*, 2016, **306**, pp. 1116–1137

[7] Dias A.A., Bezerra R.M., Pereira A.N.: 'Activity and elution profile of laccase during biological decolorization and dephenolization of olive mill wastewater', *Bioresour. Technol.*, 2004, **92**, (1), pp. 7–13

[8] Wagner C.E., Cahill T.M., Marshall P.A.: 'Extraction, purification, and spectroscopic characterization of a mixture of capsaicinoids', *J. Chem. Educ.*, 2011, **88**, (11), pp. 1574–1579

[9] Konstantinou I.K., Albanis T.A.: 'Tio_2-assisted photocatalytic degradation of azo dyes in aqueous solution: kinetic and mechanistic investigations a review', *Appl. Catal. B, Environ.*, 2004, **49**, (1), pp. 1–14

[10] Li X., Zhang Y.K., Xie Y., *ET AL.*: 'Ultrasonic-enhanced Fenton-like degradation of bisphenol a using a bio-synthesized schwertmannite catalyst', *J. Hazard. Mater.*, 2018, **344**, pp. 689–697

[11] Mollah A.H., Robinson C.W.: 'Pentachlorophenol adsorption and desorption characteristics of granular activated carbon-I. Isotherms', *Water Res.*, 1996, **30**, (12), pp. 2901–2906

[12] Hameed B.H., Din A.M., Ahmad A.L.: 'Adsorption of methylene blue onto bamboo-based activated carbon: kinetics and equilibrium studies', *J. Hazard. Mater.*, 2007, **141**, (3), pp. 819–825

[13] Ou X.X., Quan X., Chen S., *ET AL.*: 'Photocatalytic reaction by Fe (III)–citrate complex and its effect on the photodegradation of atrazine in aqueous solution', *J. Photochem. Photobiol. A.*, 2008, **197**, (2–3), pp. 382–388

[14] Zhao Y., Wang L., Fan N.N., *ET AL.*: 'Porous Zn (II)-based metal-organic frameworks decorated with carboxylate groups exhibiting high gas adsorption and separation of organic dyes', *Cryst. Growth Des.*, 2018, **18**, (11), pp. 7114–7121

[15] Liu X.P., Xiao Z.Y., Xu J., *ET AL.*: 'A NbO-type copper metal–organic framework decorated with carboxylate groups exhibiting highly selective CO_2 adsorption and separation of organic dyes', *J. Mater. Chem. A*, 2016, **4**, (36), pp. 13844–13851

[16] Hua M., Zhang S.J., Pan B.C., *ET AL.*: 'Heavy metal removal from water/wastewater by nanosized metal oxides: a review', *J. Hazard. Mater.*, 2012, **211**, pp. 317–331

[17] Neupane G., Donahoe R.J., Arai Y.: 'Kinetics of competitive adsorption/desorption of arsenate and phosphate at the ferrihydrite–water interface', *Chem. Geol.*, 2014, **368**, pp. 31–38

[18] Zhang X.M., Shen B.X., Hou X.M., *ET AL.*: 'Research on reactive adsorption desulfurization over metal oxides adsorbent', *Energy Sources A*, 2015, **37**, (2), pp. 209–216

[19] Muensri P., Danwittayakul S.: 'Removal of arsenic from groundwater using nano-metal oxide adsorbents', *Key Eng. Mater.*, 2017, **751**, pp. 766–772

[20] Bai P., Liu B., Wu P., *ET AL.*: 'Remarkably high performance of clew-like ZnO superstructure in reactive adsorption desulfurization', *Sci. China Mater.*, 2017, **60**, (10), pp. 985–994

[21] Ramezani A.H., Hoseinzadeh S., Ebrahiminejad Z.: 'Structural and mechanical properties of tantalum thin films affected by nitrogen ion implantation', *Mod. Phys. Lett. B*, 2020, **15**, (34), pp. 1–13

[22] Keshavarz A., Parang Z., Nasseri A.: 'The effect of sulfuric acid, oxalic acid, and their combination on the size and regularity of the porous alumina by anodization', *J. Nano Chem.*, 2013, **3**, (34), pp. 34–38

[23] Saadi Z., Saadi R., Fazaeli R.: 'Fixed-bed adsorption dynamics of Pb (II) adsorption from aqueous solution using nanostructured γ-alumina', *J. Nano Chem.*, 2013, **3**, (39), pp. 48–56

[24] Mohsen A., Mohammad T.G., Masoumeh T., *ET AL.*: 'Highly efcient adsorbent for removal of heavy metal ions modifed by a novel Schiff base ligand', *J. Nanostruct.*, 2018, **8**, (4), pp. 374–382

[25] Maryam A., Maziyar M.P., Hassan F.J.: 'Treatment of petrochemical wastewater by modifed electro-Fenton method with nano porous aluminum electrode', *J. Water Environ. Nanotechnol.*, 2017, **2**, (3), pp. 186–194

[26] Farahmandjou M., Golabiyan N.: 'Solution combustion preparation of nano-Al_2O_3: synthesis and characterization', *Trans. Phenom. Nano Micro Scales*, 2015, **3**, (2), pp. 100–105

[27] Elsayed A., Al-dadah R.K., Mahmoud S., *ET AL.*: 'Numerical investigation of turbulent flow heat transfer and pressure drop of Al_2O_3/water nanofluid in helically coiled tubes', *Int. J. Low-Carbon Technol.*, 2015, **10**, pp. 275–282

[28] Hoseinzadeh S., Sahebi S.A.R., Ghasemiasl R., *ET AL.*: 'Experimental analysis to improving thermosyphon (TPCT) thermal efficiency using nanoparticles/based fluids (water)', *Eur. Phys. J. Plus*, 2017, **132**, (197), pp. 2–8

[29] Samimi A., Ghadiri M., Boerefijn R., *ET AL.*: 'Effect of structural characteristics on impact breakage of agglomerates', *Powder Technol.*, 2003, **130**, pp. 428–435

[30] Islam A., Taufiq-Yap Y.H., Ravindra P., *ET AL.*: 'Development of a procedure for spherical alginate–boehmite particle preparation', *Adv. Powder Technol.*, 2013, **24**, pp. 1119–1125

[31] Fedorov A.V., Gulyaeva Y.K.: 'Strength statistics for porous alumina', *Powder. Technol.*, 2019, **343**, pp. 783–791

[32] Lv Y.M., Li D.Q., Tang P.G., *ET AL.*: 'A simple and promoter free way to synthesize spherical γ-alumina with high hydrothermal stability', *Mater. Lett.*, 2015, **155**, pp. 75–77

[33] Abdollahi A., Atashi H., Tabrizi F.F.: 'Parametric investigation of γ-alumina granule preparation via the oil-drop route', *Adv. Powder Technol.*, 2017, **28**, (5), pp. 1356–1371

[34] Ramavath P., Swathi M., Suresh M.B., *ET AL.*: 'Flow properties of spray dried alumina granules using powder flow analysis technique', *Adv. Powder Technol.*, 2013, **24**, (3), pp. 667–673

[35] Hoseinzadeh S., Ghasemiasl R., Bahari A., *ET AL.*: 'The injection of Ag nanoparticles on surface of WO_3 thin flm: enhanced electrochromic coloration efciency and switching response', *J. Mater. Sci., Mater. Electron.*, 2017, **28**, (19), pp. 14855–14863

[36] Zhang H.M., Ruan Y., Feng Y., *ET AL.*: 'Solvent-free hydrothermal synthesis of gamma-aluminum oxide nanoparticles with selective adsorption of Congo red', *J. Colloid Interface Sci.*, 2019, **536**, pp. 180–188

[37] Ramezani A.H., Hoseinzadeh S., Ebrahiminejad Z., *ET AL.*: 'Spin-polarized electron transfer in multilayers with different types of rough interfaces', *J. Supercond. Novel Magn.*, 2020, **33**, (5), pp. 1513–1519

[38] Simon C., Dirk E.: 'Investigation of the formation process of highly porous α-Al_2O_3 via citric acid-assisted sol-gel synthesis', *J. Eur. Ceram. Soc.*, 2019, **39**, (7), pp. 2493–2502

[39] Farahmandjou M., Golabiyan N.: 'New pore structure of nano-alumina (Al_2O_3) prepared by sol gel method', *J. Ceram. Process. Res.*, 2015, **16**, (2), pp. 1–4

doi: 10.1049/mnl.2020.0271